

Heidelberg-Moscow $\beta\beta$ experiment with ^{76}Ge : Full setup with five detectors

M. Günther, J. Hellmig, G. Heusser, M. Hirsch, H. V. Klapdor-Kleingrothaus,* B. Maier, H. Päs, F. Petry, Y. Ramachers, H. Strecker, and M. Völlinger
Max-Planck-Institut für Kernphysik, Heidelberg, Germany

A. Balysh, S. T. Belyaev,* A. Demehin, A. Gurov, I. Kondratenko, D. Kotel'nikov, and V. I. Lebedev
Russian Science Center Kurchatov Institute, 123 182 Moscow, Russia

A. Müller

Istituto Nazionale di Fisica Nucleare, I-67010 Assergi, Italy

(Received 20 December 1995)

The full setup of the Heidelberg-Moscow double β decay experiment is presented. This experiment gives at present the most stringent upper bound, improving the neutrino mass limit into the sub-eV range. Out of 19.2 kg of 86% enriched ^{76}Ge five crystals were grown with a total mass of 11.51 kg. Since February 1995 all five detectors, corresponding to 10.96 kg active mass, are in regular operation in the Gran Sasso underground laboratory, four of them in a common shield. No signal is observed for the neutrinoless double β decay ($0\nu\beta\beta$). The measured data from the first three enriched detectors with a statistical significance of 13.60 kg yr result in a new half-life limit of $T_{1/2}(0^+ \rightarrow 0^+) > 7.4 \times 10^{24}$ yr (90% C.L.). With this limit a Majorana mass of the neutrinos larger than 0.6 eV (90% C.L.) is excluded. From the data taken in the previously operated setup with three enriched detectors in a common shielding and a statistical significance of 10.58 kg yr new results are extracted for the two neutrino double β decay ($2\nu\beta\beta$) of ^{76}Ge . The procedure of a quantitative and model-independent description of the background via a Monte Carlo simulation is outlined in some detail. The combined result is $T_{1/2}^{2\nu} = [1.77^{+0.01}_{-0.01}(\text{stat})^{+0.13}_{-0.11}(\text{sys})] \times 10^{21}$ yr. Further on the results concerning new Majoron models and the impact on SUSY parameters are briefly reviewed. Future improvements on the background with the application of digital pulse shape analysis are discussed and an outlook on the future of $\beta\beta$ research is given. [S0556-2821(96)01523-8]

PACS number(s): 23.40.Bw, 12.60.Jv, 14.60.St

I. INTRODUCTION

The interest in neutrino physics is constantly increasing, because of the fact that physics beyond the standard model of particle physics can be probed. Several indications such as the solar ^7Be -neutrino problem, the atmospheric ν_μ deficit, and mixed dark matter models give hints of nonvanishing ν masses as predicted in grand unification theories (GUTs). These indications could be explained in GUT scenarios with degenerate neutrino masses of 0.1–2 eV [1–3].

The mass region assumed in these models can be tested in second-generation $\beta\beta$ experiments like the Heidelberg-Moscow experiment using large amounts of enriched $\beta\beta$ -emitter material and thus bring $\beta\beta$ decay into some key position in modern neutrino physics. These experiments investigate the nature of the neutrino (Majorana or Dirac particle) and give at present the most stringent limits on a nonzero Majorana neutrino mass and right-handed weak currents (RHCs). In $\beta\beta$ decay usually four decay modes are discussed [4,5]:

$$(A) \quad 2\nu\beta\beta \quad {}^Z_A X \rightarrow {}^{Z+2}_A X + 2e^- + 2\bar{\nu}_e,$$

$$(B) \quad 0\nu\beta\beta \quad {}^Z_A X \rightarrow {}^{Z+2}_A X + 2e^-,$$

$$(C) \quad 0\nu\chi\beta\beta \quad {}^Z_A X \rightarrow {}^{Z+2}_A X + 2e^- + \chi,$$

$$(D) \quad 0\nu 2\chi\beta\beta \quad {}^Z_A X \rightarrow {}^{Z+2}_A X + 2e^- + 2\chi.$$

Decay mode (A) can be understood as a process of second order Fermi theory, while the observation of the processes (B)–(D) would require physics beyond the standard model. In Fig. 1 the experimental signatures of the different decay

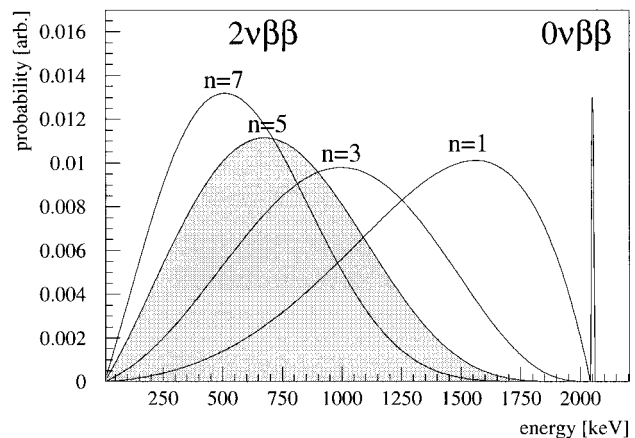


FIG. 1. Spectral shapes of the different investigated double- β decay modes; the continuous spectra are classified by their spectral index n . The spectral index for $2\nu\beta\beta$ decay is $n=5$.

*Spokesmen.

TABLE I. Technical parameters of the five enriched detectors.

Detector number	Total mass [kg]	Active mass [kg]	Enrichment in ^{76}Ge [%]	FWHM ^a at 1332 keV [keV]
enr No. 1	0.980	0.920	85.9±1.3	2.22±0.02
enr No. 2	2.906	2.758	86.6±2.5	2.43±0.03
enr No. 3	2.446	2.324	88.3±2.6	2.71±0.03
enr No. 4	2.400	2.295	86.3±1.3	2.14±0.04
enr No. 5	2.781	2.666	85.6±1.3	2.55±0.05

^aFull width at half maximum.

modes are shown for the isotope ^{76}Ge . In the case of the neutrinoless double- β decay (B) only two electrons are present in the final state of the decay, resulting in a peak at the Q value as the expected signal for detection. Since in all other decay modes additional particles are emitted, continuous spectral shapes are expected for these decay modes. To classify the different spectral shapes, the spectral index n is used, which corresponds to the power in which the energy is included in the phase space integral. The spectral index of the $2\nu\beta\beta$ decay is $n=5$.

The observation of the neutrinoless double- β $0\nu\beta\beta$ decay (B) would require massive Majorana neutrinos or a contribution of RHC's to the $0\nu\beta\beta$ amplitude. Up to now this decay mode has not been observed. Therefore an upper limit for the effective Majorana neutrino mass can be deduced from a measured half-life limit and calculated matrix elements [6]. This article will focus on the first results of the final setup of the Heidelberg-Moscow experiment with five enriched Ge detectors and the evaluation of decay modes (A) and (B). A first short announcement on these decay modes has been given in [10,11]. Furthermore, the new Majoron-accompanied neutrinoless double- β decays (C) and (D) proposed in [7] will be discussed briefly (for details see [8]).

II. EXPERIMENTAL SETUP AND MEASURED DATA

The three main advantages of the experiment are the excellent energy resolution of germanium detectors, which favors the search for the expected $0\nu\beta\beta$ peak at 2038.56 ± 0.32 keV [12], the large size of the detectors, concentrating the background in the peaks, and the fact that the source is equal to the detector, allowing large source strengths.

Overall there is 19.2 kg of enriched Ge in the Heidelberg-Moscow experiment [4,10,13–16] available with an ^{76}Ge isotopic abundance of 86% compared to 7.8% in natural Ge. Out of the raw material five p -type high-purity Ge semiconductor detectors have been built with a total mass of 11.51 kg. The enrichment we measured for each crystal separately by accelerator mass spectroscopy using residues from the crystal fabrication. All five detectors are now in regular operation in the Gran Sasso underground laboratory, which provides a shielding of 3500 meter of water equivalent (mwe). The sensitivity of this setup corresponds to an experiment with natural Ge of more than $1.2t$. The active mass of 10.96 kg is equivalent to a source strength of $125.5 \text{ mol } ^{76}\text{Ge}$ nuclei, which is at present the largest source strength of all double- β experiments. The main detector parameters are listed in Table I.

In the construction of the cryostat, mainly made of electrolytical Cu, only selected and cleaned low-level materials were used. Underground storage of these materials was applied to minimize the activation due to cosmic rays. The final assembly of the detectors is done in a clean-room environment to avoid any surface contaminations. During the installation of the detectors in the Gran Sasso laboratory, great care is taken to work close to clean-room conditions.

All detectors except detector enr No. 4 are operated in a common Pb shielding of 30 cm, which consists of an inner shielding of 10 cm radiopure LC2-grade Pb followed by 20 cm of Boliden Pb. The whole setup is placed in an air-tight steel box to build up pressure inside with radiopure nitrogen in order to suppress the ^{222}Rn contamination of the air. The steel box is centered inside a 10-cm boron-loaded polyethylene shielding to decrease the neutron flux from outside. Detector enr No. 4 is installed in a separate setup, which has an inner shielding of 27.5 cm electrolytical Cu, 20 cm lead, and boron-loaded polyethylene shielding below the steel box. To check the stability of the experiment, a calibration with a ^{228}Th and a ^{60}Co source is done weakly.

In Table II the background numbers are compared for the different data acquisition periods. The improvement from setup to setup is obvious by the decreasing background numbers. The installation of the boron-polyethylene shielding in the setup with three enriched detectors resulted in a decrease of the overall counting rate by $(7.5\pm 0.5)\%$ and in the evaluation interval of the $0\nu\beta\beta$ decay by $(22\pm 13)\%$. The performance of the chosen setup in the experiment is shown in Fig. 2 for the case of the newly installed detector enr No. 4. The effect of going deep underground and building up a suitable shielding results in a background reduction factor of four orders of magnitude in comparison to the low-level laboratory in Heidelberg with 15 mwe. Another factor of 10 is gained with the installation of the N_2 -flushing system.

Figure 3 shows the combined sum spectrum of the five enriched detectors in the Heidelberg-Moscow experiment with a statistical significance of 17.70 kg yr. All given statistical significances refer to the active mass of the experiment. Because of the large peak-to-Compton ratio of the large detectors, external γ activities are easily identified, shifting their background from the Compton continuum into the peaks. The background identified immediately by the measured γ lines in the background spectrum consists of (1) primordial activities of the natural decay chains from ^{238}U , ^{232}Th , and ^{40}K , (2) anthropogenic radio nuclides, like ^{137}Cs , and (3) cosmogenic isotopes, produced by activation due to cosmic rays. The activity of these sources in the setup is measured directly and can be located due to the measured and simulated relative peak intensities of these nuclei. Hidden in the continuous background are the contributions of (4) the bremsstrahlung spectrum of ^{210}Bi (daughter of ^{210}Pb), (5) elastic and inelastic neutron scattering, and (6) direct muon induced events.

The impact of (4) on the background spectrum is determined indirectly with a separate activity measurement, while for (5) the comparison in the measurement in the setup with three enriched detectors in a common shielding with and without neutron shielding was used. Out of the measured coincidence spectra of all detectors, the influence of muons can be estimated. External α and β activities are shielded by

TABLE III. Full data of the experiment and used data after decay of initial activities for the evaluation of the $0\nu\beta\beta$ decay.

Detector	Statistical significance [kg yr]	Statistical significance without first 200 days [kg yr]	Background 2000–2080 keV [counts/keV yr kg]
enr No. 1	3.15	2.18	0.18 ± 0.03
enr No. 2	7.87	7.02	0.20 ± 0.02
enr No. 3	5.40	4.40	0.21 ± 0.02
enr No. 4	0.93		
enr No. 5	0.35		
Σ	17.70	13.60	0.203 ± 0.014

peak counting rate. There is no contribution to the background in the interesting evaluation areas of the experiment due to this activity.

All measured background numbers will improve further on by the decay of short-lived—typical half-lives are ~ 1 yr—cosmogenic background activities inside the Ge crystal and the cryostat system. This background was produced during the exposure and transportation of the detectors at sea level by the activation through high energy cosmic radiation. The amount of activation was calculated well with the exact history of exposure and agrees within the uncertainties with the measured cosmogenic activities. With this result the influence of not directly identified isotopes can be estimated and accounts dominantly for the declining background.

Since the $2\nu\beta\beta$ spectrum is superimposed on all the background components mentioned above, it is very important to understand the exact composition of the measured background in detail. Further on, the signal-to-background ratio must be of the order of 1:1 for a clear and reliable signal detection. Fulfilling these requirements, the background can be unfolded from the measured spectrum and the result will not be effected by large uncertainties of unknown and unsure background components as in previous experiments [17,18]. For the detection of the $0\nu\beta\beta$ signal, only the achieved integral background in the expected peak area is important, because the clear signal of a line cannot be smeared out by the existing background. Here is the stability of the experiment fundamental in order to maintain the advantage of an excellent resolution of our detectors at the Q value of the $0\nu\beta\beta$ decay in the summed spectrum of all data taken. Extrapolation from the ten strongest γ lines in the background spectrum in Fig. 3 yields an energy resolution at the ground state transition of the $0\nu\beta\beta$ decay at 2038.56 keV of 3.59 ± 0.26 keV in the sum data of all five enriched detectors. This shows the good stability of the experimental parameters during the years of data acquisition when compared to the achieved detector resolutions with calibrated sources in Table I.

III. RESULTS FOR THE $0\nu\beta\beta$ DECAY

The combined spectrum for the evaluation of the $0\nu\beta\beta$ decay with 13.60 kg yr contains all data taken, except the first 200 days of measurement with each detector. These initial data of each detector were removed similar to [17], to avoid the implications of any short-lived radioactive impurities. No further cuts were applied. In Table III the statistical

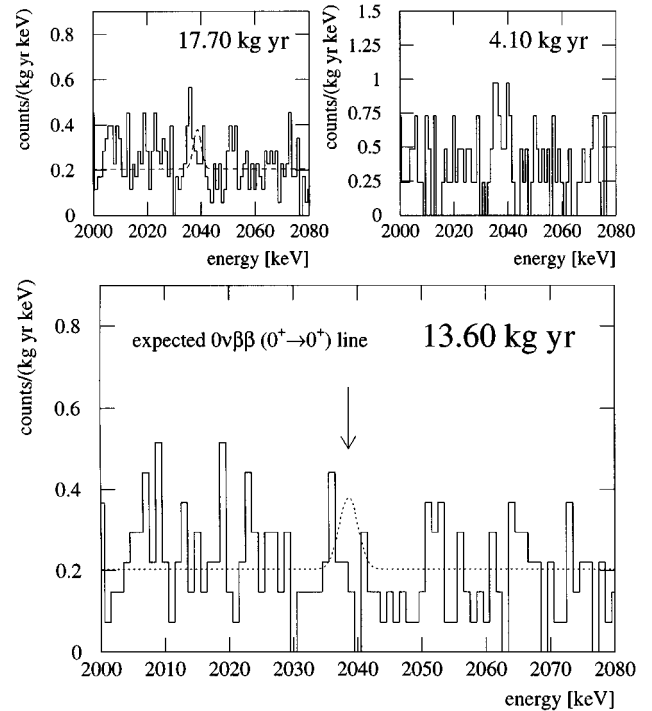


FIG. 4. Region of interest in the combined spectrum for a hypothetical $0\nu\beta\beta$ peak; the inserted curve corresponds to the excluded signal with $T_{1/2}^{0\nu} > 3.4 \times 10^{24}$ yr (90% C.L.) for all 17.70 kg yr data taken and $T_{1/2}^{0\nu} > 7.4 \times 10^{24}$ yr (90% C.L.) for 13.60 kg yr, respectively. The difference spectrum with 4.10 kg yr consists of the first 200 days of measurement of each detector.

significances of the full data and the data for the evaluation are listed. For the evaluation the symmetric energy interval 2000–2080 keV around the expected $0\nu\beta\beta$ signal is chosen. The effect of the first 200 days of data taking is clearly shown in Fig. 4. The first data of the detectors enr No. 4 and enr No. 5 will be included soon in the final evaluation, when the detectors are taking data beyond the first 200 days in the Gran Sasso laboratory.

The extrapolated resolution at the energy of the hypothetical $0\nu\beta\beta$ peak is 3.45 ± 0.29 keV in the sum spectrum of the three first detectors in the final evaluation with 13.60 kg yr. The 3σ peak interval centered at 2038.56 keV contains 23 events. With the evaluated background left and right of this interval in a 30-keV range, we expect in the peak region 23.86 ± 1.61 events. The achieved background between 2000 and 2080 keV (see Fig. 2) is 0.203 ± 0.014 [counts/keV yr kg]. Additionally the same region of the spectrum is shown for all data taken with 17.70 kg yr and the difference between these data with 4.10 kg yr.

The effect of the higher initial background activities results in a slightly higher background index and a clear structure at the decay energy. This structure is dominating in the spectrum with 4.10 kg yr, where only the first 200 days of each detector were summed up; note the different scale of the background index. This shows that the former indication of a $0\nu\beta\beta$ peak in this experiment on a 2σ level could be identified as short-lived background activities (e.g., ^{56}Co), since the real signal must be constant in time. At present we find no positive evidence for a signal of the $0\nu\beta\beta$ decay ($0^+ \rightarrow 0^+$ -transition) at 2038.56 keV.

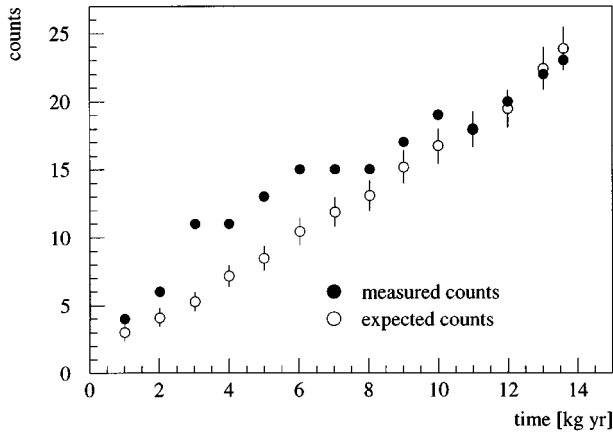


FIG. 5. Number of expected background counts (open circles with error bars) and measured total number of counts (solid circles) in the 3σ energy range of a $0\nu\beta\beta$ ($0^+ \rightarrow 0^+$) transition of ^{76}Ge as a function of measuring time.

In Fig. 5 the measured and expected number of events in the $0\nu\beta\beta$ region are shown, the latter being the measured background in the energy interval from 2000 to 2080 keV, excluding the 3σ peak region of the hypothetical $0\nu\beta\beta$ line, extrapolated into the 3σ peak region.

Since there is no signal present, we extract a half-life limit for the $0\nu\beta\beta$ decay using the method recommended by the Particle Data Group [19]. With the measured resolution and the measured background we can exclude 8.82 (5.12) events with 90% (68%) C.L., resulting in a half-life limit of

$$T_{1/2}^{0\nu} > 7.4(12.7) \times 10^{24} \text{ yr} \quad \text{with 90\% (68\%) C.L.} \quad (1)$$

To investigate the dependence of the obtained limit on the position in the spectrum, the 3σ peak interval was moved around the measured Q value at 2038.56 keV [12] between 2030 and 2048 keV. The evaluation yielded a variation of the half-life limit between 5.8 and 10.3×10^{24} yr with 90% C.L. and thus demonstrates a rather smooth background level in this energy range. The lower half-life limit of Eq. (5) is converted with the matrix elements [6] into an upper limit for the Majorana mass of the neutrinos, neglecting RHC's:

$$\langle m_\nu \rangle < 0.6(0.5) \text{ eV} \quad \text{with 90\% (68\%) C.L.} \quad (2)$$

If RHC's are included in the evaluation, we determine the following upper limits with 90% C.L.:

$$\langle m_\nu \rangle < 0.7(0.6) \text{ eV} \quad \text{with 90\% (68\%) C.L.,} \quad (3)$$

$$\langle \eta \rangle < 6.4(4.9) \times 10^{-9} \quad \text{with 90\% (68\%) C.L.,} \quad (4)$$

$$\langle \lambda \rangle < 1.1(0.8) \times 10^{-6} \quad \text{with 90\% (68\%) C.L.} \quad (5)$$

For comparison we give in Table IV a complete list of the neutrino masses obtained when using the matrix elements (given in the convention of [6,20]) of the various theoretical groups.

We see that the results essentially vary within a factor of 2 (see the discussion in [6]), with the exception of the last two cases, which, however, are ‘‘special’’ in the following sense. The calculation of Engel, Vogel, and Zirnbauer [25] is

TABLE IV. Neutrino mass limits from neutrinoless double- β decay of ^{76}Ge for different matrix elements.

Ref.	$M_{\text{GT}}^{0\nu} - M_F^{0\nu}$	$\langle m_\nu \rangle$	Comment
[6, 20]	4.186	0.56 eV	QRPA with Paris potential
[21]	4.33	0.54 eV	QRPA with Bonn potential
[22]	7.58	0.31 eV	VAMIR code
[23]	5.02	0.47 eV	shell model in weak-coupling limit
[24]	3.04	0.78 eV	QRPA, no p - n pairing
[24]	1.34	1.76 eV	QRPA, p - n pairing
[25]	1.71	1.38 eV	QRPA schematic force $\alpha' = -390 \text{ MeV}$, $g_A = 1.25$

the *only* one, which does *not* use a realistic nucleon-nucleon force, but a schematic force. The calculation of Pantis *et al.* [24] includes p - n pairing, but seems to contain still some serious inconsistencies.

By the continuous improvement of the background in the course of the experiment, the evaluated limits of the half-life for the $0\nu\beta\beta$ decay up to now show a linear dependence of time instead of the expected square root behavior. With some years of data in the full setup, the expected square root will take over. Figure 6 shows the time development up to now of the half-life limit and of the resulting Majorana neutrino mass limit with 90% C.L.

Double- β decay yields beyond information on the neutrino mass important restrictions on further parameters of beyond standard model physics, which are competitive or even more sensitive than limits from high-energy accelerators. These include SUSY models, compositeness, lept-quarks, right-handed W bosons, and others. For details we refer to [5,26,9,27,28].

IV. MONTE CARLO SIMULATION

While for the evaluation of the $0\nu\beta\beta$ signal no manipulation of the background has been done, for the evaluation of the $2\nu\beta\beta$ decay and various Majoron-emitting decay modes a detailed knowledge of the composition of the experimental background is required. All measured continuous background sources have to be taken into account in the background model, which leaves, after subtraction from the originally measured spectra, the residual spectra with the spectral shapes searched for. The measured data of the setup with three enriched detectors in a common Pb shielding between

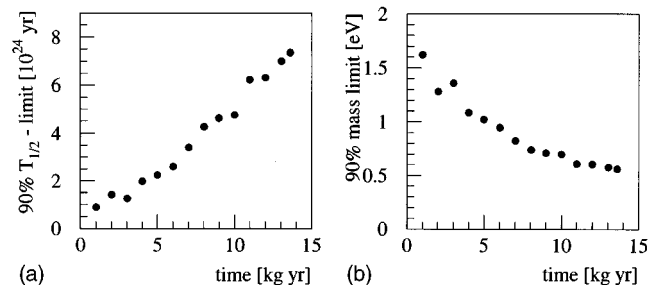


FIG. 6. Half-life limit (left) and resulting Majorana neutrino mass limit (right) with 90% C.L. for the $0\nu\beta\beta$ ($0^+ \rightarrow 0^+$) transition of ^{76}Ge as a function of measuring time.

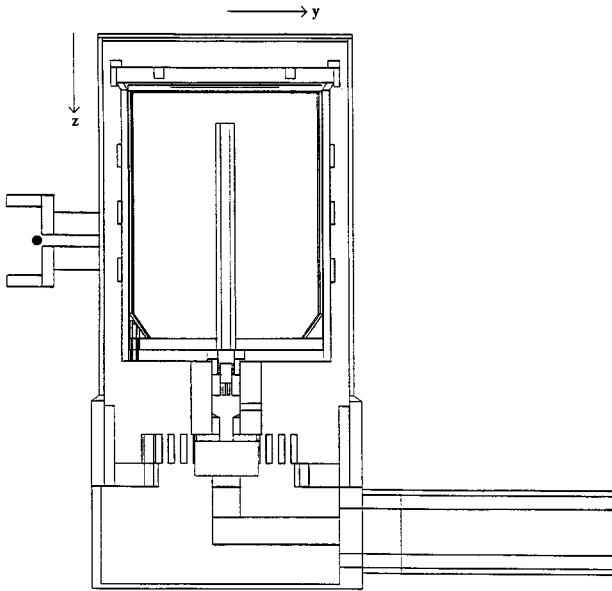


FIG. 7. Implemented geometry of a scanning measurement with a collimated ^{133}Ba source in axial direction at 9 cm below end cap of detector enr No. 2 (the source is symbolized inside the collimator with a black dot).

9/1992 and 11/1994 has been used to determine the background in detail and to achieve a more sophisticated understanding of the various background sources. The overall statistical significance of the detectors enr No. 1, enr No. 2, and enr No. 3 in this data acquisition period is 10.576 kg yr. To unfold the background a Monte Carlo background model based on the CERN code GEANT3 was developed. All radioactive sources used are available with the complete implemented decay scheme taken from [29] for the simulation. In the case of β activities the correct energy distribution of the particles is included separately, especially for the decay of ^{210}Bi . The background model consists only of measured and clearly identified background activities.

A. Calibration

The implemented geometry of the setups and detectors was tested by comparing the results with measured spectra of calibrated sources in defined locations. The deviation between simulation and measurement represents the error of the simulated detector response, caused by the code itself and small deviations in the implemented geometry in comparison to the real setup.

Each detector was scanned with a collimated ^{133}Ba source in axial (z) and radial (y) directions. The programmed geometry of such a measurement is shown in Fig. 7. The source ^{133}Ba with low-energy γ 's was chosen, because the γ beam can be collimated, the measured peak intensities are very sensitive to absorbing materials (e.g., crystalholder or inactive zone of the crystals), and the energy is mainly deposited via the photoeffect inside the crystal, giving a good spatial resolution. All measurements for the detectors enr No. 1 (15 y and 23 z measurements), enr No. 2 (14 y , 19 z), and enr No. 3 (30 y , 42 z) were simulated. For the evaluation we used the four strongest γ lines, which resulted in a combined systematical error of the simulated detector response of 7.1%

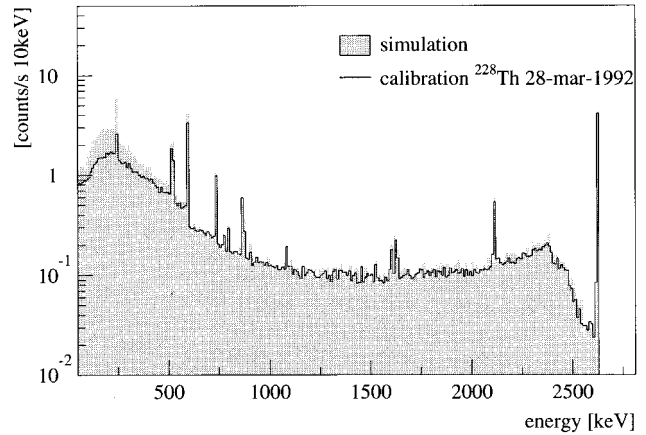


FIG. 8. Comparison of measured and simulated calibration of detector enr No. 2 within the Gran Sasso setup from 28-mar-1992.

for enr No. 1, of 5.1% for enr No. 2, and of 7.1% for enr No. 3.

To test the full energy range of natural radioactivity between 100 and 2700 keV, various other sources were simulated. As an example, an original calibration measurement in the Gran Sasso setup with ^{228}Th is compared with the simulation in Fig. 8. The agreement is quite good, although it has to be noticed that in the low-energy region the simulation gives some more events than really measured. This is explained with the uncertainty (within 2 mm) of the position of the source in the setup. In this particular case the source is partly covered by the Pb shielding; therefore, low energies are more likely to be absorbed. Above 500 keV the deviation between measurement and simulation is for the peak counting rates and the integral energy evaluation less than 10%.

Within the energy range for evaluation in this experiment, Monte Carlo simulations can be used to understand the present background in a very efficient way, which is shown with the simulated calibration measurements.

B. Background model

The measured activities in the setup are based on 47 identified γ lines in the spectra of the three enriched detectors and two separate activity measurements of ^{40}K and ^{210}Pb in the LC2-Pb. A uniform distribution of the activities inside a certain volume and material is assumed in the Monte Carlo simulation. In principle, the setup provides five major possible locations: LC2-Pb shielding, detector chamber, copper parts of the cryostats, plastic parts of the cryostats, and the Ge crystals themselves. Other materials or locations in the detectors, e.g., low-level tested steel screws or wires, are negligible, because of their small mass or volume and measured contamination levels.

The interaction and influence between each of the detectors activities with the neighboring detectors is fully included in the background model. The simulated coincidence spectra of the final background model are in good agreement with the measured coincidence spectra. This proves the validity of this approach to build up a uniform background model for three detectors simultaneously.

The simulated background spectra were not just normalized to the measured peak counting rate, because of the in-

TABLE V. Measured activities of all background components included in the uniform background model for three enriched detectors in a common shielding between 9/1992 and 11/1994 (p.d.=per detector located); the errors include the normalization and systematical misplacement errors.

Background component	Localization	Background activity [$\mu\text{Bg/kg}$]		
		enr No. 1	enr No. 2	enr No. 3
^{210}Bi bremsstrahlung	LC2-Pb		360000 ± 30000	
^{238}U decay chain	detector chamber		$126 \pm 39 \text{ mBq/m}^3$	
^{232}Th decay chain	copper p.d.	108.2 ± 12.5	16.3 ± 9.6	105.3 ± 35.7
^{54}Mn	copper p.d.	22.6 ± 5.8	16.5 ± 2.5	22.5 ± 3.3
^{57}Co	copper p.d.	20.5 ± 8.3	30.3 ± 5.0	42.1 ± 6.6
^{58}Co	copper p.d.			56.4 ± 10.8
^{60}Co	copper p.d.	92.5 ± 12.2	72.3 ± 5.2	56.0 ± 5.2
^{54}Mn	Ge crystal	4.5 ± 1.7	3.1 ± 0.9	2.5 ± 0.7
^{57}Co	Ge crystal	2.5 ± 0.8	1.4 ± 0.4	3.7 ± 0.6
^{58}Co	Ge crystal			6.1 ± 2.2
^{65}Zn	Ge crystal		6.7 ± 2.5	25.0 ± 3.6
^{40}K	LC2-Pb		271.3 ± 32.3	
^{40}K	copper enr No. 3			696.1 ± 48.1
^{137}Cs	copper p.d.	220.2 ± 24.7	65.2 ± 19.0	176.4 ± 21.3
^{207}Bi	copper p.d.	20.8 ± 11.3	4.0 ± 2.2	10.2 ± 5.5
^{125}Sb	copper p.d.	50.5 ± 18.0	20.4 ± 7.3	79.1 ± 28.2
^{134}Cs	copper p.d.	9.7 ± 14.6	4.4 ± 6.0	11.9 ± 17.9

teraction in between the detectors. To be consistent with the approach of a uniform background model, a system of linear equations for the simulated and measured peak counting rates was used to determine the correct normalization for the simulation.

The dominant background activity at energies below 500 keV is caused by ^{210}Pb contained in the inner LC2-Pb shielding, which contributes through the bremsstrahlung of its daughter ^{210}Bi (Q value=1.16 MeV). In this region almost half of the measured events are due to this contamination. The absolute activity of 0.36 ± 0.03 Bg/kg was determined separately by low-level α spectroscopy of the decay of the ^{210}Bi daughter ^{210}Po . This intrinsic activity is by far the largest contamination present in the setup. Because of this fact and the location in the large volume of the LC2-Pb shielding, this is the only component which has to be normalized to the measurement with a factor greater than 1, namely, 2.03. Since the resulting bremsstrahlung spectrum is continuous and a greater binwidth of the spectra for the evaluation is selected, the impact of the latter on deduced results is not affected by this. All other identified background activities, whose fraction in the evaluation interval is larger, are normalized with factors at least less than 0.04 to the measured spectra. Therefore the statistical errors of the simulation are negligible in comparison to the measurement.

To include the natural decay chains of ^{238}U (14 γ lines) and ^{232}Th (9 γ lines) in the background model, the peak intensities of the measured γ lines are used. Under the assumption of radioactive equilibrium and a uniform distribution of contamination, the location was determined by comparing the simulated and measured relative peak intensities. In the case of the ^{238}U decay chain, the detector chamber showed the best agreement, while for the ^{232}Th decay chain it is more realistic to locate the activity in the copper cryostat

of each detector. The error of a possible misplacement is included in the systematical error of the background model. A placement in the Ge crystal could be ruled out by the absence of any α lines in the high-energy spectra.

During the minimized exposure to the cosmic radiation when the materials were above ground, the copper of the cryostat and the Ge crystals were activated. In the measuring period the cosmogenic activities of ^{54}Mn , ^{57}Co , ^{58}Co , ^{60}Co , and ^{65}Zn are identified through their characteristic γ lines. Since most of the isotopes decay totally or partly by electron capture (EC), it is possible to distinguish between inner activities in the Ge crystal (due to the shifted γ lines with the added energy of the deexcitation x ray) and outer activities in the copper (unshifted γ lines). The measured peak intensities were used to normalize the simulated contributions to the background model.

The primordial ^{40}K content in the LC2-Pb was determined by neutron activation and is in good agreement with the measured data of enr No. 1 and enr No. 2. A second ^{40}K contamination is present in the copper of enr No. 3.

The anthropogenic activities of ^{137}Cs , ^{207}Bi , ^{125}Sb , and ^{134}Cs are surface contamination of the copper parts of the individual detectors. Because of their spectral shape, the deviation of a closer or more distant placement affects the simulated detector response not severely. To cover this uncertainty the error of a possible misplacement is again included in the systematical error.

All measured activities of the background model, given as initial activities at the beginning of the measuring period, and the localization of these contaminations are listed in Table V. To include all background components in a conservative and careful way, the individual detector contaminations are placed per detector system (p.d.=per detector located). Their spectral influence on the measured spectrum is

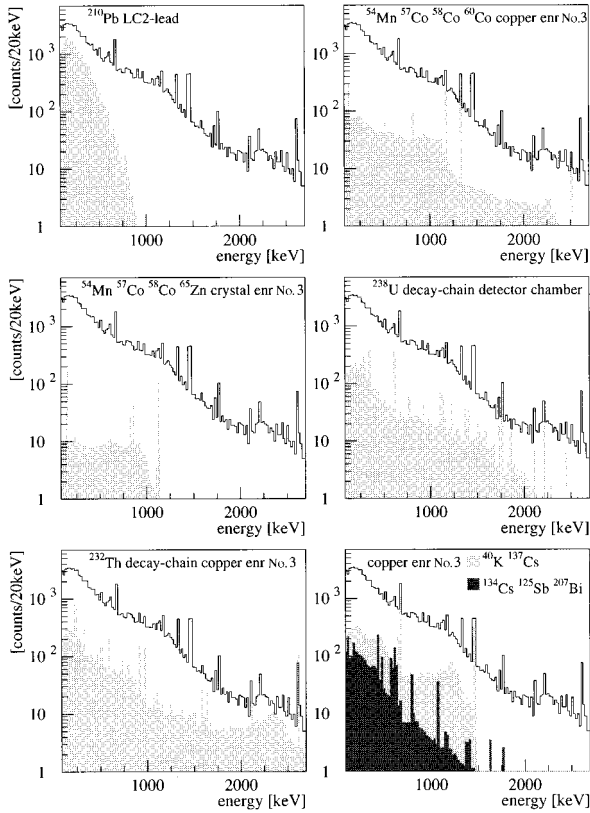


FIG. 9. The simulated background components (shaded areas) as parts of the original measured spectrum of detector enr No. 3 (solid histogram).

shown in the case of enr No. 3 in Fig. 9. The main contribution at energies below 500 keV with about 1/3 of all measured events is due to ^{210}Pb . Other significant parts of the background are caused by the natural decay chains, as well as by ^{40}K and ^{60}Co in the copper.

To avoid statistical fluctuations in the low-energy part, the evaluation interval for the $2\nu\beta\beta$ decay was chosen to be 500–2040 keV, covering 73.9% of the signal. In this way the subtraction of the background model from the original spectrum with larger errors at energies below 500 keV does not affect the results on the $2\nu\beta\beta$ decay, whose fraction on the measured events is rather small in this region. The contribution due to the located activities, e.g., in detector enr No. 3 to the spectra of enr No. 1 and enr No. 2, is shown in Fig. 10. The uniform background model includes all the influences in between the detectors.

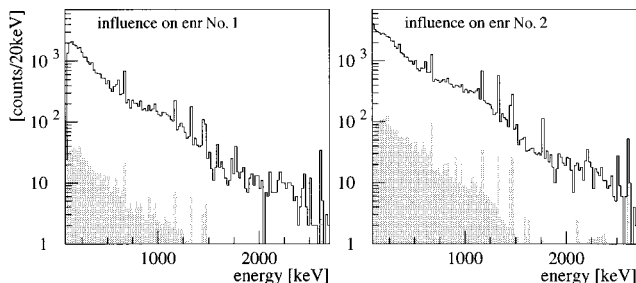


FIG. 10. Influence of activities located in detector enr No. 3 (shaded area) on the spectra of the neighboring detectors (solid histogram).

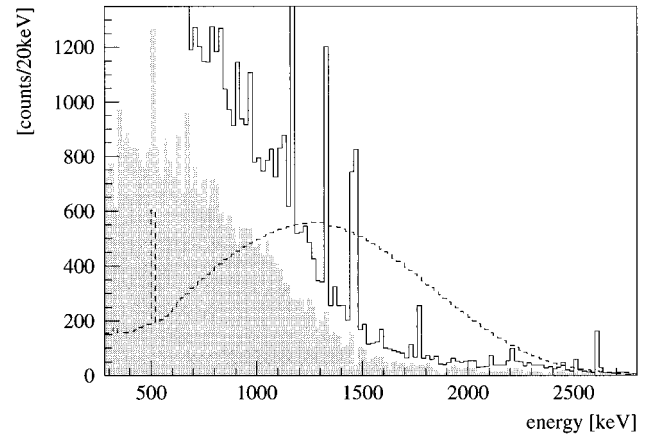


FIG. 11. Summed raw data of the three enriched detectors with a measuring time of 645 d (solid histogram), residual spectrum after subtracting all simulated background components (shaded area), and upper contribution of ^{68}Ge estimated from the 511-keV line (dashed line).

To account for the residual background due to neutrons, muons, and not directly identified background activities, a phenomenological straight line is introduced. In Fig. 11 the summed data of all three detectors are shown together with the result after subtracting all previously discussed background components. In the residual spectrum the shape of the $2\nu\beta\beta$ decay with a maximum at 700 keV is already visible. At energies above 2 MeV there are still some events left, which are due to the additional background sources mentioned above. The expected shape of all these further contributions shows in a first order approximation an increase towards low energies. To model the impact of these sources, a straight line, where the slope and intercept are determined between 2.1 and 2.8 MeV for each detector separately, is used and extended to lower energies. Overall, the contribution of this background line is 2.8% of the measured events and is consistent with the expected spectral shape of these possible background sources.

The excess of 511-keV events is treated separately. In the model only (31–50)% of the annihilation line are reproduced depending on the detector. This gives a strong hint of the influence of muons in the measurement (not explicitly simulated) and goes along with the fact that in the simulated coincidence spectra, integrally, there are slightly less events contained than there are in the measured data. Measured high-energy coincidences due to muons are not present at all in the simulated data and confirm this assumption. Out of this information the muon flux can be estimated to be of the order of the muon flux measured by the MACRO Collaboration with $2.3 \times 10^{-4} \text{ m}^{-2} \text{ s}^{-1}$ [30]. In the near future an active shielding will be placed on top of the setup to measure the effect of the muons directly in coincidence with the detectors inside.

The excess of 511-keV events can be used to derive the possible influence of ^{68}Ge in the measurement, too. ^{68}Ge can be produced by cosmic activation inside the crystals via spallation in the reaction $^{70}\text{Ge}(n,3n)^{68}\text{Ge}$. This is already strongly suppressed by the enrichment of our material in ^{76}Ge , corresponding to a deenrichment in ^{70}Ge . The still possible intrinsic contamination of ^{68}Ge could in principle con-

TABLE VI. Fraction of the background components in the evaluation interval 500–2040 keV of the $2\nu\beta\beta$ decay and the entire spectrum together with the total measured counts in these regions in $t=645$ d, the signal-to-background ($S:B$) ratio; the simulated model counts, the normalization (Δ_{norm}), and systematical misplacement error (Δ_{syst}).

Background component	Fraction					
	500–2040 keV [%]			100–2800 keV [%]		
	enr No. 1	enr No. 2	enr No. 3	enr No. 1	enr No. 2	enr No. 3
^{210}Bi bremsstrahlung	5.8	6.1	5.2	35.9	35.9	31.3
^{238}U decay chain	9.5	9.1	7.9	8.7	8.1	7.1
^{232}Th decay chain	8.9	2.1	9.6	9.2	2.2	9.8
^{54}Mn copper	0.7	0.8	0.7	0.4	0.5	0.5
^{57}Co copper				0.2	0.4	0.4
^{58}Co copper			0.6			0.5
^{60}Co copper	10.7	12.7	6.8	5.3	6.8	3.6
^{54}Mn Ge crystal	0.4	0.5	0.3	0.2	0.2	0.1
^{57}Co Ge crystal				0.2	0.1	0.3
^{58}Co Ge crystal			0.2			0.1
^{65}Zn Ge crystal		0.5	1.3		0.2	0.6
^{40}K LC2-Pb	7.0	7.6	6.4	3.7	4.3	3.5
^{40}K copper enr No. 3			5.8			3.5
^{137}Cs	6.7	3.5	6.4	6.6	3.2	6.0
^{207}Bi	1.7	0.6	1.0	1.3	0.4	0.7
^{125}Sb	0.5	0.4	1.0	1.4	0.9	2.4
^{134}Cs	0.7	0.5	1.0	0.5	0.4	0.7
511-keV line	0.4	0.6	0.9	0.1	0.2	0.3
straight line	5.3	5.7	5.5	2.5	3.0	2.8
influence on enr No. 1		2.7	1.5		2.7	1.4
influence on enr No. 2	2.0		1.8	1.7		1.5
influence on enr No. 3	2.2	4.2		2.2	3.9	
overall counts	9924	22268	25096	32803	65699	74480
$S:B$	1:1.66	1:1.37	1:1.78	1:4.0	1:2.8	1:3.4
model counts	6195	12854	16071	26272	48262	57356
Δ_{norm}	345	521	704			
Δ_{syst}	132	525	456			

tribute to the measurement via the decay of its daughter ^{68}Ga with a Q value of 2.921 MeV. The only evident signature of this background source is the characteristic x ray with 10.4 keV. The present settings of the thresholds of the detectors do not allow one to measure this line. Assuming that all excess events are due to ^{68}Ge , meaning the β^+ decay of ^{68}Ga , the resulting contribution is shown in Fig. 11. This estimate is obviously in contradiction with the measured data. Therefore we conclude that no significant contributions to the $2\nu\beta\beta$ background from ^{68}Ge are present and give the following upper bounds, determined for each detector separately: 6 $\mu\text{Bq/kg}$, for enr No. 1, 0.1 $\mu\text{Bq/kg}$ for enr No. 2, and 54 $\mu\text{Bq/kg}$ for enr No. 3. It has to be mentioned that part of the excess of the 511-keV line might be explained with a ^{106}Ru contamination (especially via the 511-keV γ line from the decay of the daughter nuclei ^{106}Rh) with a half-life of 386 d; making the previously obtained limits conservative.

The fraction in percent of 19 different background components on the total measured spectrum in the evaluation interval and the entire spectrum is given in Table VI. The total number of events measured in 645 d serving as 100% is also listed together with the signal-to-background ratio

($S:B$): 1:1.7 for enr No. 1, 1:1.4 for enr No. 2, and 1:1.8 for enr No. 3. The $S:B$ ratio is evaluated under the assumption that all events not explained by the background model are due to $2\nu\beta\beta$ decay. These ratios are slightly lower than in [10], because the peaks, with a rather significant fraction of counts, are included in this evaluation, whereas before the $S:B$ ratio was only determined for the continuous parts of the spectrum. Finally, the normalization error and systematical misplacement uncertainty are given for the model per detector. A very sensitive test for the model was performed with the comparison of the simulated and measured coincidence spectra. All lines and the spectral shapes (despite the effect due to muons) are reproduced within the errors and confirm the validity of the uniform background model. The overall model consists of 19 different background components, which are located in 46 distinct locations and produce in total 132 simulated detector-specific spectra.

C. Results for the $2\nu\beta\beta$ decay

The bin width of the spectra was chosen to be 20 keV per channel to avoid statistical fluctuations when subtracting

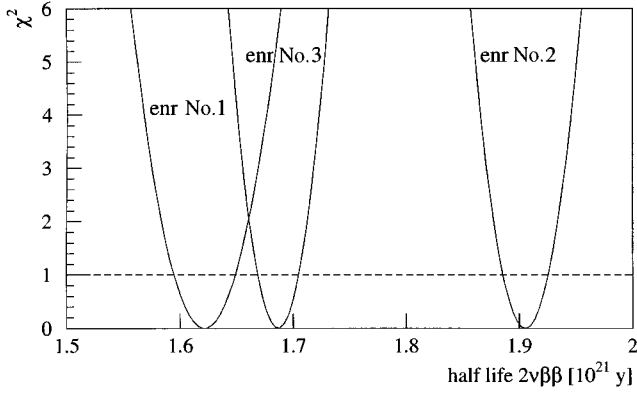


FIG. 12. Resulting χ^2 distribution out of the maximum-likelihood fit for the evaluation of the $2\nu\beta\beta$ decay in the residual spectra after subtraction of the background of the three enriched detectors (the dotted line corresponds to the 68% error).

simulated γ lines from the measured spectra. It is assumed for this evaluation that the resulting difference of the measured and simulated background spectra contains only the $2\nu\beta\beta$ signal.

The result of a maximum-likelihood fit of the data and the theoretically expected $2\nu\beta\beta$ spectrum then results in the following half-lives for the three detectors with 68% C.L.:

$$T_{1/2}^{2\nu}(\text{No. 1}) = [1.62_{-0.03}^{+0.03}(\text{stat})_{-0.14}^{+0.18} \times (\text{norm})_{-0.06}^{+0.07}(\text{syst})_{-0.11}^{+0.13}(\text{sim})] \times 10^{21} \text{ yr}, \quad (6)$$

$$T_{1/2}^{2\nu}(\text{No. 2}) = [1.91_{-0.02}^{+0.02}(\text{stat})_{-0.10}^{+0.12} \times (\text{norm})_{-0.10}^{+0.12}(\text{syst})_{-0.10}^{+0.12}(\text{sim})] \times 10^{21} \text{ yr}, \quad (7)$$

$$T_{1/2}^{2\nu}(\text{No. 3}) = [1.69_{-0.02}^{+0.02}(\text{stat})_{-0.14}^{+0.17} \times (\text{norm})_{-0.08}^{+0.10}(\text{syst})_{-0.10}^{+0.13}(\text{sim})] \times 10^{21} \text{ yr}. \quad (8)$$

The statistical error originates from the parabolic behavior of the logarithmic likelihood ratio, which corresponds to a χ^2 function [32], which is shown in Fig. 12 for the three detectors. With the normalization error due to the errors of the measured area of the γ lines, the systematic misplacement error of background activities, and the error of the simulated detector response, all possible implications to the result are included. The result for the detector enr No. 2 is shown in Fig. 13.

The combined result for the three detectors with the uniform background model with 68% C.L. is

$$T_{1/2}^{2\nu} = [1.77_{-0.01}^{+0.01}(\text{stat})_{-0.11}^{+0.13}(\text{syst})] \times 10^{21} \text{ yr}. \quad (9)$$

For comparison two former results for the $2\nu\beta\beta$ decay are shown in Fig. 13, too. The obtained result is slightly higher than in [10] with $(1.42_{-0.13}^{+0.13}) \times 10^{21}$ yr, because the interaction of the detectors between each other was not taken into account in this earlier result of the Heidelberg-Moscow experiment. The curve with $(0.92_{-0.04}^{+0.07}) \times 10^{21}$ yr from [17], which is corrected to $(1.2_{-0.1}^{+0.2}) \times 10^{21}$ yr in [33], still deviates sig-

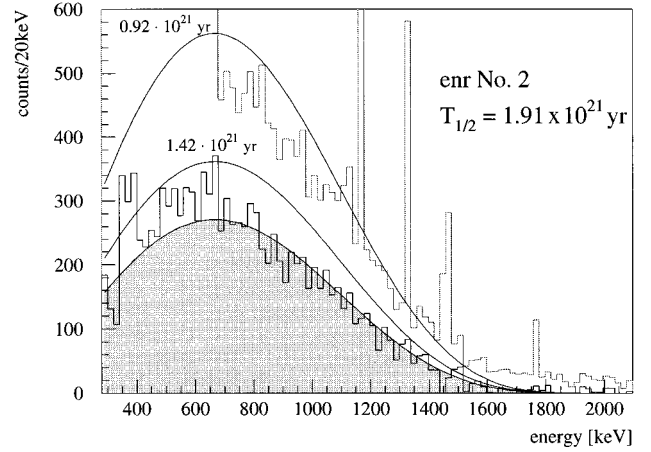


FIG. 13. Result for the evaluation of the $2\nu\beta\beta$ decay of ^{76}Ge in detector enr No. 2: original spectrum (dotted histogram), residual spectrum after subtraction of background model (solid histogram), and fitted $2\nu\beta\beta$ spectrum (shaded area); for comparison, two former $2\nu\beta\beta$ results are shown [10,17].

nificantly from the result presented here, because the background assumptions made in this experiment were only qualitative and incomplete.

The presence of isotopes inside crystals like ^{68}Ge and ^{90}Sr with $Q=2.284$ MeV of its daughter ^{90}Y and ^{234m}Pa with $Q=2.29$ MeV, which might in principle influence or even simulate a $2\nu\beta\beta$ signal [10], is excluded by the spectral shape and end point of their continuous simulated spectra [31]. These sources do not have significant γ lines from which they could be identified. In the case of ^{77}Ge and ^{60}Co in the crystal and other cosmogenics, the spectral shape does not fit at all and the calculations of the production via cosmic rays show in no case significant contributions, while all measured cosmogenic activities are reproduced within the errors.

The expected constant integral counting rate in the evaluation interval for the resulting spectra after background subtraction was tested and confirmed for 20 points of time during the measuring period. Based on the uniform background model and the determined activities in Table V for each point of time, the background model was calculated backwards, corresponding to the measured spectra at this time. In order to investigate the $2\nu\beta\beta$ counting rate in between two time points, the previously measured spectra and background model are subtracted from the result of the given time point. The difference between measured data and background model then gives the specific $2\nu\beta\beta$ counting rate in between two time points. The result is shown in Fig. 14 for each detector separately and summarized for all three enriched detectors together.

In spite of the statistical fluctuations in the time development of the $2\nu\beta\beta$ counting rates in the data of each detector, the expected constant stability for the investigated signal can be seen. Combining the detectors, thus reducing the statistical errors, the effect of the installation of the neutron shielding after 383 d in this measuring period is obvious, too (compare Table II). Overall, we have 5.56 ± 0.24 $2\nu\beta\beta$ events per [d] and [kg] active Ge crystal, corresponding to a half-life of $T_{1/2} = 1.74 \times 10^{21}$ yr. Taking only the first 14 time points up to the installation of the neutron shielding with 5.84 ± 0.30

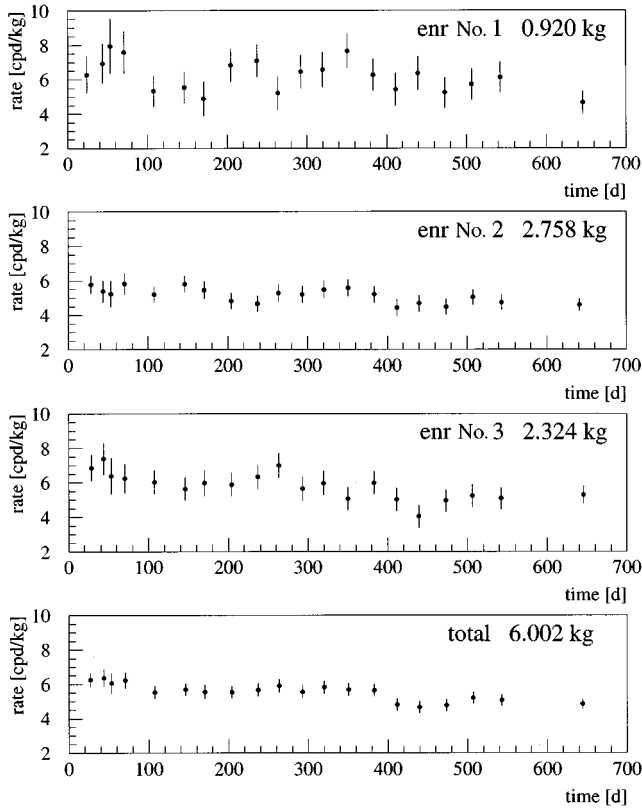


FIG. 14. Time development of the $2\nu\beta\beta$ counting rate in the evaluation interval 500–2040 keV after subtraction of the background model for 20 time intervals for each detector separately, and summarized.

$2\nu\beta\beta$ events counts/d [(cpd)/kg], a half-life of $T_{1/2}=1.65\times 10^{21}$ yr is deduced, while the last 260 d on its own gives 4.91 ± 0.20 $2\nu\beta\beta$ events [(cpd)/kg] and a half-life of $T_{1/2}=1.97\times 10^{21}$ yr. The latter result is certainly not correct, since the influence of the straight line was calculated linearly back in time, although it is expected that the slope of this straight line has decreased in the measuring phase with neutron shielding. Therefore the half-life is overestimated.

In order to avoid this complication, the whole evaluation of the $2\nu\beta\beta$ decay was performed again only for the time the neutron shielding was installed. The background activities were calculated back to this time point and normalized to the spectra. A new phenomenological straight line was adapted to this part of data, which showed, as expected, a smaller slope as evaluated in the full set of data. The result of the maximum-likelihood fit yields the following half-lives for the $2\nu\beta\beta$ decay with 68% C.L.: for enr No. 1 $[1.63^{+0.03}_{-0.03}(\text{stat})^{+0.25}_{-0.19}(\text{syst})]\times 10^{21}$ yr, for enr No. 2 $[1.96^{+0.02}_{-0.02}(\text{stat})^{+0.23}_{-0.18}(\text{syst})]\times 10^{21}$ yr, and for enr No. 3 $[1.78^{+0.02}_{-0.02}(\text{stat})^{+0.27}_{-0.21}(\text{syst})]\times 10^{21}$ yr. All these deduced half-lives are slightly larger than the ones evaluated in the total measuring time. Especially in the case for enr No. 3, the half-life is longer, because this detector was installed new in this measuring period, but the initial cosmogenic activities have decayed by the time the neutron shielding was installed. Within the errors these results approve the results deduced before, even giving hints of a slightly longer half-life. Since the results here are still dependent on the overall uniform background model, the previous obtained half-lives are decisive.

TABLE VII. Different majoron modes, their leptonic charge, spectral index n , and the new bounds on the half-life and coupling constants derived in this work (from [8]).

Modus	GB	L	n	$T_{1/2}>(90\% \text{ C.L.})$	$g<(90\% \text{ C.L.})$
$\beta\beta\phi$	no		1	7.91×10^{21}	2.3×10^{-4}
$\beta\beta\phi$	yes		1	7.91×10^{21}	2.3×10^{-4}
$\beta\beta\phi$	no	-2	1	7.91×10^{21}	2.3×10^{-4}
$\beta\beta\phi$	yes	-2	3	5.85×10^{21}	0.18
$\beta\beta\phi\phi$	gauge boson	-2	3	5.85×10^{21}	0.18
$\beta\beta\phi\phi$	yes and no		3	5.85×10^{21}	4.1
$\beta\beta\phi\phi$	no	-1	3	5.85×10^{21}	4.1
$\beta\beta\phi\phi$	yes	-1	7	6.64×10^{21}	3.3

The Heidelberg-Moscow experiment reached with 21 115 $2\nu\beta\beta$ events in the evaluation interval of 500–2040 keV the highest statistics of all all $\beta\beta$ experiments for the direct detection of the $2\nu\beta\beta$ decay mode. With a detailed understanding of all major background components, the evaluation is not dependent on any cuts applied to the measured data, unlike the case of other experiments. Actually, the raw data are used for a full background consideration.

D. Results for the Majoron decay

In the ordinary Majoron model [34], the Majoron is a massless scalar Goldstone boson, which is associated with the spontaneous breaking of $B-L$ symmetry and the existence of Majorana masses of the neutrinos. In this framework only the singlet Majoron is still possible, since doublet and triplet Majorons are ruled out by the CERN electron e^+e^- collider LEP [35] by the measured width of the Z^0 resonance. Nevertheless, ‘‘fine-tuning’’ is required for the singlet Majoron to be consistent with the existing bounds on neutrino masses and to still preserve an observable rate for Majoron-emitting double- β decays.

Therefore new Majoron models have been invented avoiding the unnatural ‘‘fine-tuning’’ [7]. In these models the terminus Majoron stands in a more general sense for a light or massless boson coupling to neutrinos. The new properties of these Majorons are that they can carry units of leptonic charge, that there can be Majorons which are not Goldstone bosons and that decays with the emission of two Majorons can occur. The last case can be fermion mediated or scalar mediated, although only for fermion-mediated decays is a contribution to double- β decay expected [7,8].

In Table VII all considered models are listed with their leptonic charge and spectral shape index n of the sum energy of the emitted electrons (see Fig. 1, $n=1$ corresponds to the singlet Majoron). The spectral index is defined from the phase space of the emitted particles, $G\sim(Q_{\beta\beta}-T)^n$, where $Q_{\beta\beta}$ is the Q value of the decay and T the sum energy of the two electrons.

For the evaluation of the half-life limits, the data of the detector enr No. 2 was used with the corresponding background model previously discussed. This detector was chosen, because of its size and the best background of all detectors. In order to cover all Majoron modes sufficiently and to minimize the systematic errors of the background model an evaluation interval of 300–2040 keV was selected. With a

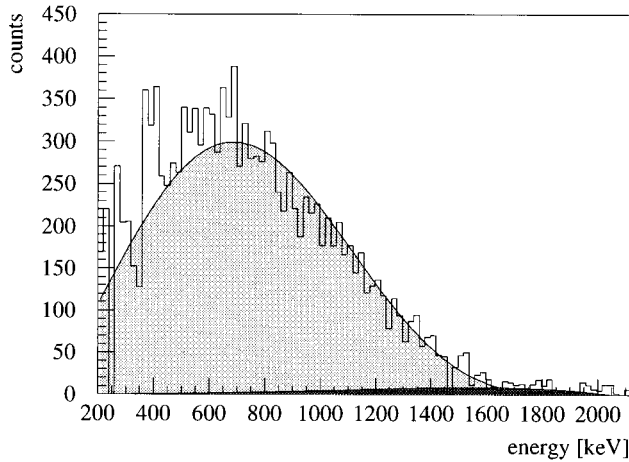


FIG. 15. “Ordinary Majoron” ($n=1$) in the area of fit: 300–2040 keV, yielding a half-life bound of $T_{1/2} > 7.91 \times 10^{21}$ yr with (90% C.L.).

simultaneous maximum-likelihood fit of the $2\nu\beta\beta$ decay and one Majoron-emitting decay, the half-life limits given in Table VII were determined.

The result of the data fit for the ordinary Majoron with $n=1$ is, for example, shown in Fig. 15. The experimental spectrum is shown as a histogram, while the light-grey-shaded area is the best fit for the $2\nu\beta\beta$ decay. The dark-shaded area corresponds to the Majoron.

It has to be mentioned that the deviation from zero of the Majoron-emitting modes is, for $n=1$, 0.29σ , for $n=3$, 0.90σ , and for $n=7$, 0.35σ , while the result for the $2\nu\beta\beta$ decay is consistent within the errors with the evaluation mentioned in the previous section. The $2\nu\beta\beta$ half-life extracted in all two-parameter fits varies in the 1σ range of the result obtained in an exclusive $2\nu\beta\beta$ decay evaluation.

With the matrix elements and phase spaces given in [8], the evaluated half-life limits can be converted into upper limits for the various effective Majoron neutrino coupling constants (see Table VII). Note that the surprisingly weak limits obtained for all of the new Majoron models are caused by the small values of the corresponding nuclear matrix elements and phase spaces and are independent of the isotope under consideration [8]. The limits for the new Majoron modes were deduced for the first time.

V. OUTLOOK

A. Digital pulse shape analysis

For the first time a new method of digital pulse shape analysis (DPSA) with the new enriched detector enr No. 5 has been applied [36]. This reduces the background described above further by a considerable factor.

The idea of this electronic approach is to decrease the number of background counts based on the search for characteristic variations, due to different interaction mechanisms of the incident radiation, in the course of the preamplifier output pulse. The DPSA in Ge detectors is capable of distinguishing between single-site events (SSE), which deposit energy locally at one site in the crystal, and multiple site events (MSE's), which are spread out over the entire volume of the detector. Examples of the first class are a single Compton-

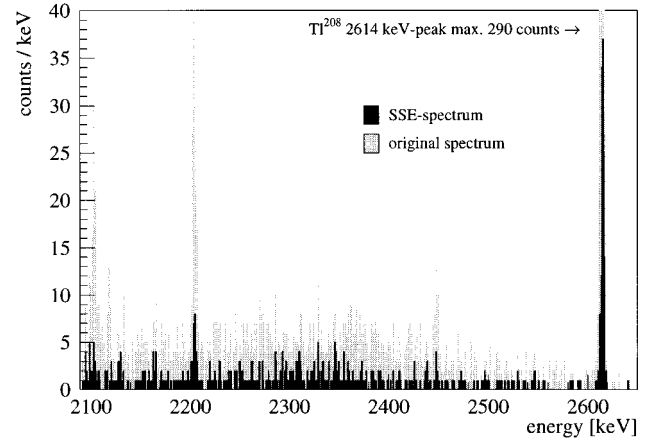


FIG. 16. Comparison of a background spectrum from the detector enr No. 5 measured without any shielding between 2090 and 2650 keV and the derived SSE spectrum. The SSE spectrum contains integral a factor of 4 less counts than the original spectrum. The 2614-keV peak of ^{208}Tl has a peak maximum of 290 counts in the original spectrum (taken from [31]).

scattered escape event and the interaction of a β particle because of the small range of electrons in the crystal.

In the experiment the signal of a $0\nu\beta\beta$ event is a SSE, while the background is characterized by MSE's due to multiple Compton scattering in this energy region. The developed DPSA [36] was tested with regular Ge detectors before it was finally installed and checked with the new detectors enr No. 5. In Fig. 16 a background spectrum of enr No. 5, measured in Heidelberg without any further shielding, and the resulting SSE energy spectrum after the application of DPSA are depicted. The integral number of counts in the Compton region between 2260 and 2360 keV in the original spectrum is 1462 counts and 315 counts in the remaining SSE spectrum. This is an improvement of about a factor of 5. The peak at 2614 keV is not removed completely due to the effect that 10% of the MSE's appear like SSE's and the deviation of DPSA from maximum reachable discrimination efficiency. The discrimination efficiency has been determined to be 80% [37]. It is difficult to derive a general quantity which characterizes the improvement obtainable with DPSA, since it is dependent on the composition of the background.

The measurement with DPSA applied to enr No. 5 in the Gran Sasso underground laboratory started in February 1995 in the setup with four enriched detectors. The first data show a discrimination factor for the background similar to that in Heidelberg. From the in total 15 measured counts in the energy range of 2000–2080 keV within 155.9 kg d with detector enr No. 5, only two counts remain after switching on the DPSA, one at precisely the energy of (2038.8 ± 3.6) keV [36]. Further measurements will show whether this event is a real $0\nu\beta\beta$ candidate.

In general, we can expect that an improvement of the half life limit for $0\nu\beta\beta$ decay by at least a factor of 2 can be obtained with the application of DPSA. This would allow, provided in all detectors DPSA would be installed, with the present setup to reach in 1 year a half-life limit for $0\nu\beta\beta$ decay of about 2×10^{25} yr.

B. Future and conclusion

The Heidelberg-Moscow experiment is the now the *only* $\beta\beta$ experiment exploring the sub-eV range for the mass of the neutrinos. With five enriched detectors with a total mass of 11.51 kg operated in the Gran Sasso underground laboratory, the experiment has reached its final setup. The experiment will probe within about 5 years the neutrino mass down to ~ 0.2 eV.

The best presently existing limits besides the Heidelberg-Moscow experiment, obtained with the isotopes ^{48}Ca [38], ^{82}Se [39], ^{100}Mo [40], ^{116}Cd [41], ^{130}Te [42], ^{136}Xe [43], and ^{150}Nd [44], with half-life limits above 10^{21} yr, are shown in Fig. 17.

Other double- β decay setups presently under construction or partly in operation such as NEMO [45], the Gotthard ^{136}Xe TPC experiment [46], the ^{130}Te cryogenic experiment [42], a new ELEGANT ^{48}Ca experiment using 64 g of ^{48}Ca [47], a hypothetical experiment with an improved UCI TPC [44] assumed to use 1.6 kg of ^{136}Xe , etc., will not reach or exceed the ^{76}Ge limits. As pointed out recently by Raghavan [48], even the use of an amount of about 200 kg of enriched ^{136}Xe or 2 tons of natural Xe added to the scintillator of the Kamiokande detector or similar amounts added to BOR-EXINO (both primarily devoted to solar neutrino investigation) would hardly lead to a sensitivity larger than the present ^{76}Ge experiment. An interesting future candidate might be a ^{150}Nd bolometer exploiting the relatively large phase space of this nucleus (see [44]). The way outlined by [49] proposing a TPC filled with 1 ton liquid-enriched ^{136}Xe and identification of the daughter by laser fluorescence may not be feasible in a straightforward way.

It is obvious that the Heidelberg-Moscow experiment will give the sharpest limit for the electron neutrino mass for the next decade. For further improvements beyond the region of < 0.1 eV, one has to think of *very large* experiments with *much larger* source strength.

Concluding second-generation $\beta\beta$ experiments have, after the introduction of new interpretations of the problems of solar and atmospheric neutrinos and of dark matter, involving degenerate neutrino mass scenarios, reached a key position in modern neutrino physics. They will be able to check these new interpretations in the not too far future. The Heidelberg-Moscow experiment has reached a leading position among these new $\beta\beta$ experiments and as the first of them now yields results in the sub-eV range.

ACKNOWLEDGMENTS

This work was supported by the Bundesministerium für Forschung und Technologie der Bundesrepublik Deutschland, the State Committee of Atomic Energy of Russia, and

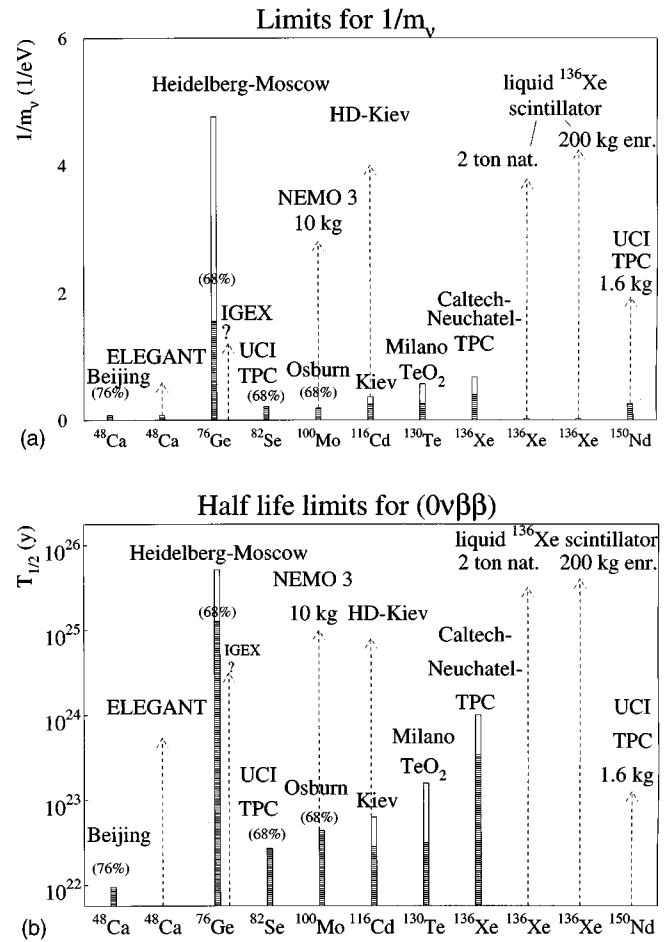


FIG. 17. Present situation, 1995, and expectation for the near future until the year 2000 and beyond, of the most promising $\beta\beta$ experiments concerning accessible half-life (a) and neutrino mass limits (b). The solid bars correspond to the present status, open bars correspond to “safe” expectations for the year 2000, and dashed lines correspond to long-term planned or hypothetical experiments.

the Istituto Nazionale di Fisica Nucleare of the Italian Republic. The generous support of Professor E. Belotti, Professor N. Cabibbo, Professor L. Maiani, and Professor P. Monacelli is gratefully acknowledged. The authors want to thank Dr. T. Raudorf of EG&G Ortec for good cooperation and Professor V. Prusakov and his co-workers for performing the isotope separation. M.H. was supported by the Deutsche Forschungsgemeinschaft (Grant No. 446 JAP-113/101/0 and KI 253/8-1). B.M. was supported by the Human Capital and Mobility program of the European Community (Grant No. ERBCHBGCT928183).

- [1] D. G. Lee and R. N. Mohapatra, Phys. Lett. B **329**, 463 (1994).
- [2] S. T. Petcov and A. Smirnov, Phys. Lett. B **322**, 109 (1994).
- [3] A. Ioannissyan and J. W. F. Valle, Phys. Lett. B **332**, 93 (1994).
- [4] H. V. Klapdor-Kleingrothaus, Prog. Part. Nucl. Phys. **32**, 261

- (1994); H. V. Klapdor-Kleingrothaus, in *Proceedings of the IV International Symposium on Weak and Electromagnetic Interaction in Nuclei (WEIN'95)*, Osaka, Japan, 1995, edited by H. Ejiri, T. Kishimoto, and T. Sato (World Scientific, Singapore, in press), p. 174.

- [5] H. V. Klapdor-Kleingrothaus and A. Staudt, *Non-Accelerator Particle Physics* (IOP, Bristol, 1995).
- [6] A. Staudt, K. Muto, and H. V. Klapdor-Kleingrothaus, *Europhys. Lett.* **13**, 31 (1990).
- [7] C. P. Burgess and J. M. Cline, *Phys. Rev. D* **49**, 5925 (1994); P. Bamert, C. P. Burgess, and R. N. Mohapatra, *Nucl. Phys. B* **449**, 25 (1995).
- [8] M. Hirsch, H. V. Klapdor-Kleingrothaus, S. G. Kovalenko and H. Päs, *Phys. Lett. B* **372**, 8 (1996); J. Hellmig *et al.*, in *Proceedings of the International Workshop on Double Beta Decay and Related Topics*, edited by H. V. Klapdor-Kleingrothaus and S. Stoica (World Scientific, Singapore, 1996).
- [9] M. Hirsch, H. V. Klapdor-Kleingrothaus, and S. G. Kovalenko, *Phys. Rev. Lett.* **75**, 17 (1995); *Phys. Lett. B* **352**, 1 (1995); M. Hirsch, H. V. Klapdor-Kleingrothaus, and S. G. Kovalenko, *Phys. Rev. D* **53**, 1329 (1996).
- [10] Heidelberg-Moscow Collaboration, A. Balysh *et al.*, *Phys. Lett. B* **322**, 176 (1994).
- [11] Heidelberg-Moscow Collaboration, A. Balysh *et al.*, *Phys. Lett. B* **356**, 450 (1995).
- [12] J. G. Hykawy *et al.*, *Phys. Rev. Lett.* **67**, 1708 (1991).
- [13] H. V. Klapdor-Kleingrothaus, Internal Report No. MPI-H-1987-V 17 (Proposal), Heidelberg, 1987 (unpublished).
- [14] Heidelberg-Moscow Collaboration, A. Balysh *et al.*, *Phys. Lett. B* **283**, 32 (1992).
- [15] Heidelberg-Moscow Collaboration, M. Beck *et al.*, *Phys. Rev. Lett.* **70**, 2853 (1993).
- [16] Heidelberg-Moscow Collaboration, M. Beck *et al.*, *Phys. Lett. B* **336**, 141 (1994).
- [17] F. T. Avignone *et al.*, *J. Phys. G* **17**, 181 (1991).
- [18] A. A. Vasenko *et al.*, *Mod. Phys. Lett. A* **5**, 1299 (1990).
- [19] Particle Data Group, J. J. Hernández *et al.*, *Phys. Lett. B* **239**, 1 (1990).
- [20] K. Muto, E. Bender, and H. V. Klapdor, *Z. Phys. A* **334**, 187 (1989).
- [21] T. Tomoda and A. Faessler, *Phys. Lett. B* **199**, 475 (1987).
- [22] T. Tomoda, A. Faessler, K. W. Schmid, and F. Grümmer, *Nucl. Phys. A* **452**, 591 (1986).
- [23] W. C. Haxton and G. J. Stephenson, *Prog. Part. Nucl. Phys.* **12**, 409 (1984).
- [24] G. Pantis, F. Simkovic, J. D. Vergados, and A. Faessler, *Phys. Rev. C* **53**, 695 (1996).
- [25] J. Engel, P. Vogel, and M. R. Zirnbauer, *Phys. Rev. C* **37**, 731 (1988).
- [26] *Proceedings of the International Workshop on Double Beta Decay and Related Topics* [8].
- [27] M. Hirsch, H. V. Klapdor-Kleingrothaus, and S. G. Kovalenko, *Phys. Lett. B* **378**, 17 (1996); **352**, 1 (1995).
- [28] M. Hirsch, H. V. Klapdor-Kleingrothaus, and S. G. Kovalenko, *Phys. Rev. D* **54**, R4207 (1996); *Phys. Rev. Lett.* **17**, 75 (1995); *Phys. Rev. D* **53**, 1329 (1996); *Phys. Lett. B* **372**, 181 (1996).
- [29] *Nuclear Data Sheets* (Academic Press, Duluth, MN).
- [30] MACRO Collaboration, H. C. de Marzo *et al.*, *Nucl. Instrum. Methods Phys. Res. A* **314**, 380 (1992).
- [31] B. Maier, Ph.D. thesis, University of Heidelberg, 1995.
- [32] S. Baker and R. D. Cousins, *Nucl. Instrum. Methods Phys. Rev. A* **221**, 437 (1984).
- [33] F. T. Avignone *et al.*, *Prog. Part. Nucl. Phys.* **32**, 223 (1994).
- [34] Y. Chikashige, R. N. Mohapatra, and R. D. Peccei, *Phys. Rev. Lett.* **45**, 1926 (1980); *Phys. Lett.* **98B**, 265 (1981).
- [35] J. Steinberger, *Phys. Rep.* **203**, 345 (1991).
- [36] F. Petry, H. V. Klapdor-Kleingrothaus, and B. Maier (unpublished); F. Petry, Ph.D. thesis, University of Heidelberg, 1995.
- [37] J. Hellmig, Ph.D. thesis, University of Heidelberg, 1996; Hellmig *et al.* (unpublished).
- [38] Ke You *et al.*, *Phys. Lett. B* **265**, 53 (1995).
- [39] S. R. Elliott *et al.*, *Phys. Rev. C* **46**, 1535 (1992).
- [40] M. Alston-Garnjost *et al.*, *Phys. Rev. Lett.* **71**, 831 (1993).
- [41] F. A. Danevich *et al.*, *Phys. Lett. B* **344**, 72 (1995).
- [42] A. Alessandrello *et al.*, *Phys. Lett. B* **335**, 519 (1994).
- [43] J.-C. Vuilleumier *et al.*, *Phys. Rev. D* **48**, 1009 (1993).
- [44] M. K. Moe *et al.*, *Prog. Part. Nucl. Phys.* **32**, 247 (1994); M. K. Moe *et al.*, in *Neutrino 94*, Proceedings of the 16th International Conference on Neutrino Physics and Astrophysics, Eilat, Israel, edited by A. Dar *et al.* [*Nucl. Phys. B (Proc. Suppl.)* **38**, 36 (1995)].
- [45] NEMO Collaboration, D. Lalanne *et al.*, in *TAUP 93*, Proceedings of the Third International Workshop on Theoretical and Phenomenological Aspects of Underground Physics, Assergi, Italy, edited by C. Arpesella *et al.* [*Nucl. Phys. B (Proc. Suppl.)* **35**, 369 (1994)].
- [46] V. Jörgens *et al.*, in *TAUP 93*, p. 378.
- [47] K. Kume *et al.*, ELEGANT Collaboration, in *Proceedings of the International Workshop on Double Beta Decay and Related Topics* [8].
- [48] R. S. Raghavan, *Phys. Rev. Lett.* **72**, 1411 (1994).
- [49] M. K. Moe, *Phys. Rev. C* **44**, R931 (1991).